Multi-octave spectral beam combiner on ultra-broadband photonic integrated circuit platform

Eric J. Stanton,* Martijn J. R. Heck, Jock Bovington, Alexander Spott, and John E. Bowers

[1]*Electrical and Computer Engineering Department, University of California, Santa Barbara California 93106, USA*
*estanton@ece.ucsb.edu

Abstract: We present the design of a novel platform that is able to combine optical frequency bands spanning 4.2 octaves from ultraviolet to mid-wave infrared into a single, low M^2 output waveguide. We present the design and realization of a key component in this platform that combines the wavelength bands of 350 nm – 1500 nm and 1500 nm – 6500 nm with demonstrated efficiency greater than 90% in near-infrared and mid-wave infrared. The multi-octave spectral beam combiner concept is realized using an integrated platform with silicon nitride waveguides and silicon waveguides. Simulated bandwidth is shown to be over four octaves, and measured bandwidth is shown over two octaves, limited by the availability of sources.

©2015 Optical Society of America

OCIS codes: (130.3120) Integrated optics devices; (140.3298) Laser beam combining.

References and links

1. B. G. Lee, J. Kansky, A. K. Goyal, C. Pflügl, L. Diehl, M. A. Belkin, A. Sanchez, and F. A. Capasso, "Beam combining of quantum cascade laser arrays," Opt. Express **17**(18), 16216–16224 (2009).
2. A. A. Kosterev and F. K. Tittel, "Chemical sensors based on quantum cascade lasers," IEEE J. Quantum Electron. **38**(6), 582–591 (2002).
3. I. H. White, "A multichannel grating cavity laser for wavelength division multiplexing applications," J. Lightwave Technol. **9**(7), 893–899 (1991).
4. L. Wang, C. Tong, H. Peng, and J. Zhang, "High power semiconductor laser beam combining technology and its applications," Proc. SPIE **8796**, 87961N (2013).
5. F. Silva, D. R. Austin, A. Thai, M. Baudisch, M. Hemmer, D. Faccio, A. Couairon, and J. Biegert, "Multi-octave supercontinuum generation from mid-infrared filamentation in a bulk crystal," Nat. Commun. **3**, 807 (2012).
6. E. J. Bochove, "Theory of spectral beam combining of fiber lasers," IEEE J. Quantum Electron. **38**(5), 432–445 (2002).
7. V. Daneu, A. Sanchez, T. Y. Fan, H. K. Choi, G. W. Turner, and C. C. Cook, "Spectral beam combining of a broad-stripe diode laser array in an external cavity," Opt. Lett. **25**(6), 405–407 (2000).
8. C. D. Stacey, C. Stace, and R. G. Clarke, "Ultrabroadband spectral beam combiner spanning over three octaves," Appl. Opt. **52**(29), 7200–7205 (2013).
9. H. H. Chang, Y. H. Kuo, R. Jones, A. Barkai, and J. E. Bowers, "Integrated hybrid silicon triplexer," Opt. Express **18**(23), 23891–23899 (2010).
10. J. T. Bovington, M. J. R. Heck, and J. E. Bowers, "Heterogeneous lasers and coupling to Si□N□ near 1060 nm," Opt. Lett. **39**(20), 6017–6020 (2014).
11. A. W. Fang, H. Park, O. Cohen, R. Jones, M. J. Paniccia, and J. E. Bowers, "Electrically pumped hybrid AlGaInAs-silicon evanescent laser," Opt. Express **14**(20), 9203–9210 (2006).
12. A. Spott, M. L. Davenport, J. Peters, J. T. Bovington, M. J. Heck, J. E. Bowers, and J. R. Meyer, "A CW mid-infrared hybrid silicon laser at room temperature," in *Proceedings of IEEE Photonics Conference* (2014), paper PD 1.
13. M. J. R. Heck, J. F. Bauters, M. L. Davenport, J. K. Doylend, S. Jain, G. Kurczveil, S. Srinivasan, Y. Tang, and J. E. Bowers, "Hybrid silicon photonic integrated circuit technology," IEEE J. Sel. Top. Quantum Electron. **19**(4), 6100117 (2013).
14. D. Dai, Z. Wang, J. F. Bauters, M. C. Tien, M. J. Heck, D. J. Blumenthal, and J. E. Bowers, "Low-loss Si3N4 arrayed-waveguide grating (de)multiplexer using nano-core optical waveguides," Opt. Express **19**(15), 14130–14136 (2011).
15. G. Kurczveil, M. J. R. Heck, J. D. Peters, J. M. Garcia, D. Spencer, and J. E. Bowers, "An integrated hybrid silicon multiwavelength AWG laser," IEEE J. Sel. Top. Quantum Electron. **17**(6), 1521–1527 (2011).
16. J. F. Bauters, M. L. Davenport, M. J. R. Heck, J. K. Doylend, A. Chen, A. W. Fang, and J. E. Bowers, "Silicon on ultra-low-loss waveguide photonic integration platform," Opt. Express **21**(1), 544–555 (2013).

#230667 - $15.00 USD Received 16 Jan 2015; revised 20 Mar 2015; accepted 20 Mar 2015; published 22 Apr 2015
© 2015 OSA

17. M. Piels, J. F. Bauters, M. L. Davenport, M. J. R. Heck, and J. E. Bowers, "Low-loss silicon nitride AWG demultiplexer heterogeneously integrated with hybrid III–V/silicon photodetectors," J. Lightwave Technol. **32**(4), 817–823 (2014).
18. R. Soref, "Mid-infrared photonics in silicon and germanium," Nat. Photonics **4**(8), 495–497 (2010).
19. A. Gorin, A. Jaouad, E. Grondin, V. Aimez, and P. Charette, "Fabrication of silicon nitride waveguides for visible-light using PECVD: a study of the effect of plasma frequency on optical properties," Opt. Express **16**(18), 13509–13516 (2008).
20. R. A. Soref, S. J. Emelett, and W. R. Buchwald, "Silicon waveguided components for the long-wave infrared region," J. Opt. A, Pure Appl. Opt. **8**(10), 840–848 (2006).
21. J. F. Bauters, M. J. R. Heck, D. John, D. Dai, M. C. Tien, J. S. Barton, A. Leinse, R. G. Heideman, D. J. Blumenthal, and J. E. Bowers, "Ultra-low-loss high-aspect-ratio Si3N4 waveguides," Opt. Express **19**(4), 3163–3174 (2011).
22. A. F. Milton and W. K. Burns, "Tapered velocity couplers for integrated optics: design," Appl. Opt. **14**(5), 1207–1212 (1975).
23. X. Sun, H. C. Liu, and A. Yariv, "Adiabaticity criterion and the shortest adiabatic mode transformer in a coupled-waveguide system," Opt. Lett. **34**(3), 280–282 (2009).
24. L. A. Coldren, S. W. Corzine, and M. L. Mašanović, *Diode Lasers and Photonic Integrated Circuits* (John Wiley & Sons, 2012), Chap. 6.
25. Z. Wang and D. Dai, "Ultrasmall Si-nanowire-based polarization rotator," J. Opt. Soc. Am. B **25**(5), 747–753 (2008).

1. Introduction

Integrated spectral beam combining technologies for high power broadband light sources enable technologies such as integrated spectroscopy systems [1,2] and wide-band wavelength division multiplexing [3]. New high performance broadband technologies are also important for developments in free space communications, remote sensing, medical radiation therapy, and a host of other applications [4]. Current competitive technologies for high power broadband sources with low M^2 output use supercontinuum generation [5] or spectral beam combining [6]. Supercontinuum generation requires a high power pump to generate output through nonlinear processes. Such sources have output power and bandwidth limited by the pump power and require components that are challenging to integrate. Existing spectral beam combining technologies use free space optics to externally combine laser array output beams [7], but only narrow bandwidths are achieved. To cover multi-octave bandwidths, separate discrete laser sources are used [8].

By integrating spectral beam combining components along with multi-spectral laser sources on a single photonic chip, a broadband and scalable power source can be realized with the advantages of photonic integration, including reduced cost, compact size, and high efficiency. Existing integration technologies cannot provide multi-spectral light generation and low loss beam combining in a single photonic chip. Different gain materials and mechanisms must be used to generate UV to mid-IR wavelengths with integrated lasers, specifically between 350 nm and 6500 nm for the application of this work. Also, no single waveguide platform practically provides low loss waveguides and spectral beam combining components across this multi-octave bandwidth. To address these challenges, we propose using multiple die bonding [9] for heterogeneous integration to create multi-spectral laser sources on chip and two waveguide designs for long and short wavelength regimes. Heterogeneous integration of light sources has been demonstrated on silicon spanning very-near-infrared (VNIR) [10], near-infrared (NIR) [11], and mid-infrared (mid-IR) [12]. The hybrid silicon and III-V/Si_3N_4 on silicon platforms enable such a broad spectrum of sources to be processed on a single chip [13].

The multi-octave spectral beam combiner that is proposed in this work uses three stages of spectral combining: intra-band, inter-band, and ultra-broadband combining as shown in Fig. 1. Here we define a band as the range of wavelengths, for example the UV, visible (UV), VNIR, NIR, and mid-IR bands. The intra- and inter-band stages utilize common integrated photonic architectures, but the final ultra-broadband stage involves a novel approach to combine long and short wavelength regimes to a single output. By ensuring maximum fundamental mode excitation, the output will have the highest beam quality, defined by a low M^2 value, spanning multiple octaves. The M^2 value is ratio to the output beam divergence to a diffraction limited beam divergence. Further details of the multi-octave spectral beam combiner design and the

#230667 - $15.00 USD Received 16 Jan 2015; revised 20 Mar 2015; accepted 20 Mar 2015; published 22 Apr 2015
© 2015 OSA

fabrication, experimental testing, and analysis of the ultra-broadband combiner are covered in this paper. We show low insertion loss spectral beam combining for wavelengths spanning more than two octaves. The ultra-broadband combiner is the key element for the integrated multi-octave spectral beam combiner. Its design and demonstration shows that the entire platform is now feasible. Integrated high power and broadband light source applications in spectroscopy and communications can now be realized with the multi-octave spectral beam combiner.

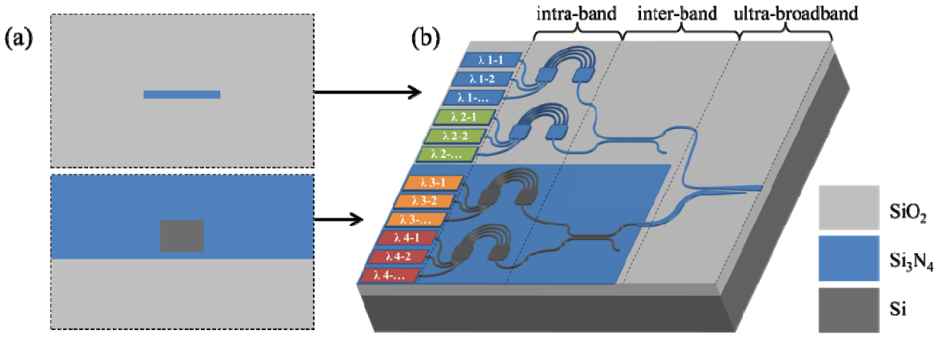

Fig. 1. (a) Cross-sectional view of the waveguide types: silicon nitride (top) and silicon (bottom). (b) Schematic design of multi-octave spectral beam combiner with integrated laser array with multiple lasers labeled "X" and each spectral band labeled "Y" formatted "λ X-Y".

We begin in Section 2 by detailing the design of the multi-octave spectral beam combiner including the ultra-broadband combiner. In Section 3 and 4 we present the experimental setup and measurement results. Finally, in Section 5 we discuss the results and compare simulation data to the experimental testing data.

2. Multi-octave spectral beam combiner

2.1 Platform and waveguides

The multi-octave spectral beam combiner, in Fig. 1(b), is designed to be compatible with multiple arrays of heterogeneously integrated diode lasers where each laser operates at a different wavelength and each array covers a different spectral band. A first stage of intra-band combiners multiplexes light with arrayed waveguide gratings (AWG's) [14,15], to combine each laser output within a spectral band into a single single-mode waveguide. A second stage of directional couplers is used to combine all of the spectral bands within each waveguide type. Before the final ultra-broadband combiner stage, optical modes in the silicon core waveguide are transferred to the silicon nitride core waveguide [16,17]. The two waveguides resulting from each waveguide platform are then inputs to the ultra-broadband combiner.

Using two waveguide types avoids prohibitively high material losses that would be present in a single waveguide platform for UV to mid-IR wavelengths while providing a platform compatible with heterogeneous integration of laser sources covering the same spectral range. Waveguide geometries can either be dual layer buried rib type, as in Fig. 2(a), or a single layer buried channel type, as is Fig. 2(b), in order to manage waveguide modes and increase the tolerance of the waveguide effective index against process variations, respectively. Adiabatic tapers, also shown in Fig. 2, transition between waveguide types. For this design, wavelengths longer than 1.5 μm are guided by a silicon core with silicon nitride cladding waveguide and wavelengths shorter than 1.5 μm are guided by a silicon nitride core with silicon dioxide cladding waveguide. The motivation for the dual waveguide platform is to provide an ultra-broadband spectral transparency from UV to mid-IR. We avoid silicon absorption in the VNIR, VIS, and UV bands by using silicon nitride and silicon dioxide (down to ~350nm) and we avoid silicon dioxide absorption in the mid-IR band (up to ~6.5 μm) by using silicon and silicon nitride [18,19]. Significant mid-IR optical absorption in

#230667 - $15.00 USD Received 16 Jan 2015; revised 20 Mar 2015; accepted 20 Mar 2015; published 22 Apr 2015
© 2015 OSA

silicon dioxide increases loss after the transition from the silicon waveguide to the silicon nitride waveguide, both shown in Fig. 1(a), but it is feasible to minimize the waveguide length and keep absorption loss less than 1 dB. Other approaches could be used to avoid absorption loss, for example by etching away the silicon dioxide underneath the silicon nitride, leading to a membrane type waveguide [20]. For mid-IR wavelengths in the silicon nitride core waveguide, silicon substrate leakage also contributes significant loss. Although substrate leakage loss is not addressed in this work, we plan to investigate undercut etching the silicon substrate below the silicon nitride waveguide platform in regions that guide mid-IR light. This reduces substrate leakage loss for mid-IR wavelengths and it should not affect loss at shorter wavelengths.

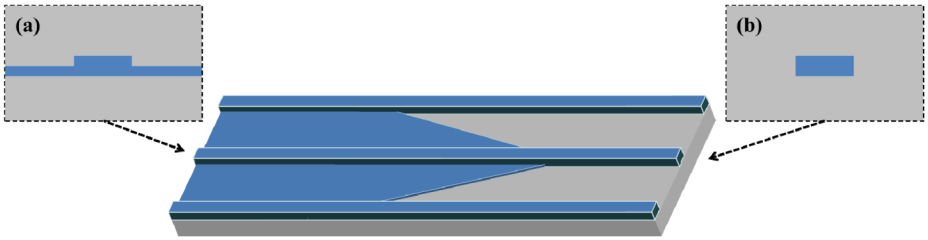

Fig. 2. Example of an adiabatic taper from a buried Si_3N_4 rib (a) to buried channel (b) type waveguide. Facet cross-sections show the partially etched waveguide on the left and fully etched waveguide on the right. The top SiO_2 cladding shown in the facet cross-sections is not shown in the taper diagram.

The silicon nitride waveguide platform must ultimately guide light across the entire UV to mid-IR spectrum for the ultra-broadband combiner stage and the final output waveguide. Therefore, this waveguide platform must also provide low loss for NIR to mid-IR wavelengths as well as UV to NIR wavelengths. By employing a high aspect ratio of width to thickness, the sidewall scattering loss can be minimized [21]. Substrate leakage and material absorption losses for mid-IR wavelengths can be minimized as previously discussed through silicon substrate undercut and minimizing the length of the final ultra-broadband combiner and output waveguide region.

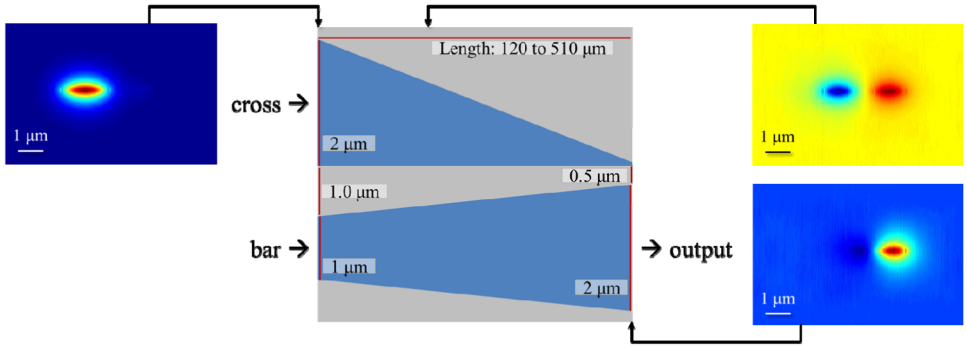

Fig. 3. Ultra-broadband combiner schematic. Blue color represents 200 nm tall Si_3N_4 and the grey color represents SiO_2, which also clads the Si_3N_4 by 2 μm above and below. Transverse mode profiles are shown at three different positions along the BPM simulated propagation.

2.2 Ultra-broadband combiner design

The ultra-broadband combiner design is based on the adiabatic tapered mode coupler [22], but it also includes a tapered coupler gap to decrease the total coupler length. Analysis of the structure in Fig. 3, shows that there is a short wavelength spectrum and long wavelength spectrum of high TE fundamental mode transmission for the bar and cross inputs, respectively. The long wavelength cross input operates similarly to the previously

#230667 - $15.00 USD Received 16 Jan 2015; revised 20 Mar 2015; accepted 20 Mar 2015; published 22 Apr 2015
© 2015 OSA

demonstrated adiabatic coupling devices [22,23], but the short wavelength bar input propagates light that does not have high enough coupling strength to be perturbed by the inversely tapering waveguide from the cross input. The TE fundamental mode transmission trend shows a cross-over wavelength where the transmission from each input is equivalent. Wavelengths longer than this cross-over wavelength have high transmission through the cross input and wavelengths shorter than the cross-over wavelength have high transmission through the bar input.

Previous examples of adiabatic couplers, as in [22,23], approach the design with a theoretical model treating the waveguide propagation constant as slowly varying along the coupler length. For this ultra-broadband combiner, a theoretical modal would need to include propagation constants with a finite derivative with respect to the propagation distance since previously derived expressions do not agree with the performance of this coupler. Therefore, beam propagation method (BPM) simulation software was used to design this coupler and predict coupling efficiency trends versus coupler length and wavelength.

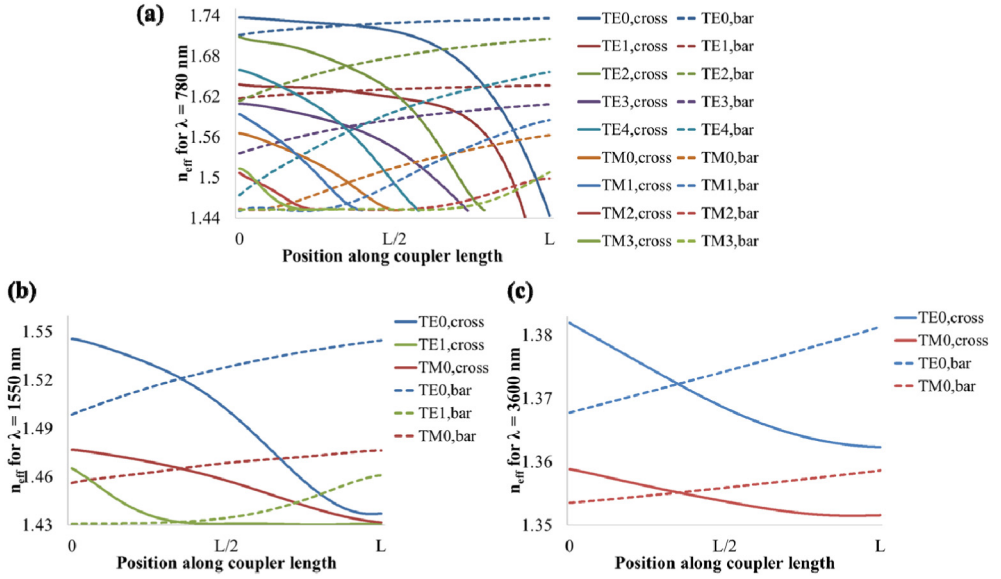

Fig. 4. Effective indices in the bar (dashed lines) and cross (solid lines) waveguides of the ultra-broadband combiner as a function of position along the coupler length for (a) 780 nm, (b) 1550 nm, and (c) 3600 nm. Each position along the coupler length corresponds to the tapered bar and cross waveguide widths as shown in Fig. 3.

The primary design tradeoff for such a broadband device is to choose waveguide geometries that guide the longest wavelengths without excessive loss and guide the shortest wavelengths while minimizing the number of guided modes. Considering that the application of this device involves an array of integrated diode lasers, any of the diode laser wavelengths will preferably lase into the fundamental TE mode [24]. Therefore, even though the input waveguide may support TM modes and higher order TE modes, it is assumed that only the fundamental TE is excited. Similarly, other laser sources for mid-IR light, such as interband cascade lasers (ICLs) or quantum cascade lasers (QCLs), also lase in a fundamental mode, either TE or TM, and a fundamental TM mode can be rotated to a fundamental TE polarized mode [25]. The guided mode eigenvalues for 780 nm, 1550 nm, and 3600 nm wavelengths are shown in Fig. 4 for the cross and bar waveguides of the ultra-broadband combiner as a function of position along the coupler's length.

The wavelengths that we use in our measurements are chosen to evaluate the three wavelength regimes of interest: high transmission of short wavelengths (VNIR), transmission near the cross-over wavelength (NIR), and high transmission of long wavelengths (mid-IR).

#230667 - $15.00 USD Received 16 Jan 2015; revised 20 Mar 2015; accepted 20 Mar 2015; published 22 Apr 2015
© 2015 OSA

Along the length of the coupler, propagation constant β matching between coupling waveguides occurs for various modes as shown in Fig. 4. Strong coupling between modes is achieved with β matching, high percentage modal overlap, and slowly varying β along the coupler length. For high fundamental mode transmission from each input the short wavelength bar input should not be perturbed along the coupler and the cross input should completely couple into the output waveguide. The β matching between the 780 nm fundamental modes in Fig. 4(a) occurs when the modal overlap is low so the overall coupling is low. For 1550 nm, the modal overlap is higher in the β matching region and some coupling occurs. The largest 3600 nm mode has a high mode overlap and high coupling occurs where there is β matching.

Since the coupler will have decreased fundamental mode transmission near the cross-over wavelength, this wavelength regime is not an ideal operating point. This work investigates the parameters that affect the cross-over wavelength to enable engineering of a particular cross-over wavelength by measuring transmission for various lengths of the ultra-broadband combiner and three wavelength spectra in the NIR: 1310 nm, 1430 nm, and 1550 nm.

To experimentally test the ultra-broadband combiner the fundamental TE mode must be excited for each input and wavelength. An input mode filter is designed in the fabricated devices with partially etched waveguides to minimize higher order TE mode excitation. Light is coupled into the cross and bar inputs via partially etched waveguides at the facets, which are adiabatically tapered to fully etched waveguides of 2 μm and 1 μm widths for the cross and bar inputs, respectively, to the ultra-broadband coupler as shown in Fig. 5. At the labeled region "I", the bar and cross inputs at the facet are initially 0.4 μm and 2.0 μm wide partially etched waveguides, respectively, in order to minimize higher order mode excitation. Next, at region "II", the buried rib waveguide adiabatically tapers to a buried channel waveguide as in Fig. 2. At region "III" the 0.4 μm wide waveguide is then laterally tapered to a 1.0 μm wide waveguide for the input to the ultra-broadband combiner. The cross waveguide is already the appropriate 2.0 μm width after the bi-level taper in region "II" so there is not another lateral taper for this waveguide.

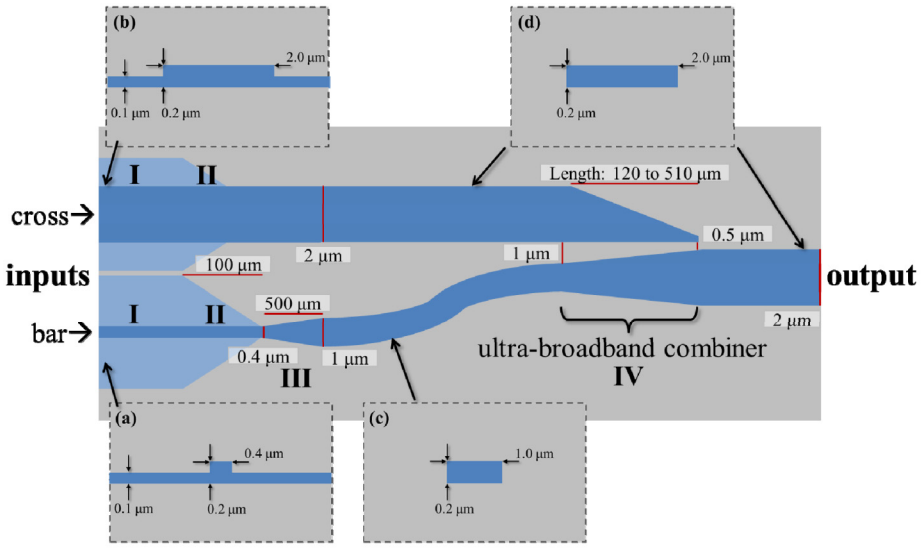

Fig. 5. Ultra-broadband combiner and input tapered waveguide schematic. Light blue color represents 100 nm tall Si_3N_4 and blue color represents 200 nm tall Si_3N_4.

The guided mode eigenvalues in region "I" of Fig. 5 for 780 nm, 1550 nm, and 3600 nm wavelengths are shown in Table 1. TM mode excitation is avoided by polarization filtering at the input. Since the 1550 nm cross input has a TE1 mode, it is incorporated in the BPM simulations. All other waveguides do not guide higher order TE modes for these wavelengths.

#230667 - $15.00 USD Received 16 Jan 2015; revised 20 Mar 2015; accepted 20 Mar 2015; published 22 Apr 2015
© 2015 OSA

Table 1. Effective indices and bi-level taper transmission[a] for applicable wavelengths of each input waveguide.

		Effective Indices			Bi-level Taper Transmission (Region "II")					
					Input: TE0			Input: TE1		
Waveguide	λ (nm)	TE0	TE1	TM0	TE0	TM0	TE1	TE0	TM0	TE1
bar input (a)	780	1.66	-	1.57	100.0%	0.0%	-	-	-	-
	1550	1.49	-	1.46	94.1%	0.0%	-	-	-	-
cross input (b)	1550	1.55	1.50	1.48	100.0%	0.0%	0.0%	0.0%	91.4%	8.6%
	3600	1.39	-	-	-	-	-	-	-	-

[a]Simulations are performed with Photon Design's FIMMWAVE and FIMMPROP software.

For the bi-level taper in region "II" of Fig. 5, the TE mode transmission is also shown in Table 1. The TM mode excitation is not shown since the TE modes can be efficiently excited with high polarization extinction ratio, which is discussed further in Section 3. The 3600 nm taper transmission is not shown since this input taper is removed for 3600 nm transmission simulations and measurements since it is not necessary to isolate the fundamental TE mode and only adds more loss.

The taper in region "III" of Fig. 5 is completely adiabatic and simulations show no loss for each mode present in the bar waveguide.

The ultra-broadband combiner, shown in region "IV" of Fig. 5, linearly tapers each waveguide along the length of the coupler. The width of the cross input tapers from 2 μm to 100 nm, which is the narrowest achievable taper width with the deep-UV lithography process used here, and the width of the bar input tapers from 1 μm to 2 μm. The coupler gap is tapered from 1 μm to 0.5 μm.

2.3 Ultra-broadband combiner BPM transmission simulations

In Fig. 6 we show simulation trends we have obtained with BPM simulation software for fundamental mode transmission as a function of wavelength and coupler length. A 3D semi-vectorial BPM simulation is set up for each wavelength with refractive indices following the Sellmeier equation with coefficients A1 = 2.8939 and B1 = 0.13967 for silicon nitride and A1 = 0.6961663, B1 = 0.0684043, A2 = 0.4079426, B2 = 0.1162414, A3 = 0.8974794, and B3 = 9.896161. The simulation window size varies as a function of wavelength from 14.5 μm to 70 μm in the horizontal direction and 4.5 μm to 16 μm in the vertical direction. Similarly, the step size in each transverse direction increases from 0.005 μm to 0.1 μm and in the propagation direction from 0.01 μm to 0.2 μm. The smaller window and step sizes correspond to the shortest wavelength of 350 nm and increase with wavelength to the largest window and step size for the longest wavelength of 6500 nm.

We investigated the cross-over wavelength trend for various coupler lengths and see a trend of red-shifted cross-over wavelength while decreasing the coupler length. A variety of other factors, such as coupler gap, taper rate, material indices, waveguide geometries, and modal excitation, also affect the cross-over wavelength, but these are not varied. The coupler length is most easily controllable parameter that can provide the widest range of cross-over wavelength tuning. To achieve cross-over wavelengths outside of this tuning range, the coupler gap and taper rate can also be easily tuned, but this is not investigated in this work.

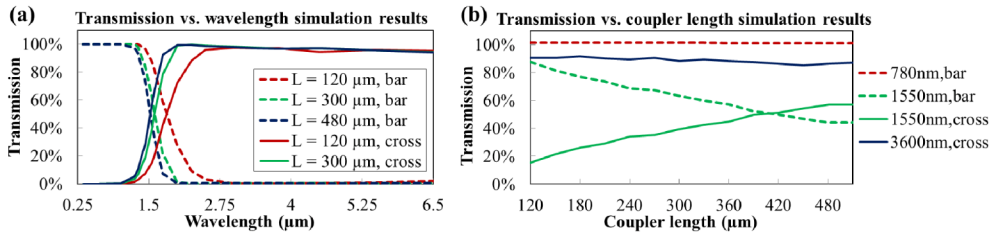

Fig. 6. Simulations of fundamental mode (a) transmission vs. wavelength and (b) transmission vs. coupler length.

#230667 - $15.00 USD Received 16 Jan 2015; revised 20 Mar 2015; accepted 20 Mar 2015; published 22 Apr 2015
© 2015 OSA

This simulated device was fabricated and tested as shown in section 4. Mode excitation and measurement is a critical issue for (V)NIR wavelengths since multiple TE modes exist in the bar waveguide. In order to simulate and measure fundamental mode transmission the performance of the higher order TE mode must be characterized so the measurement setup can be designed to represent the fundamental mode transmission. The TE0 and TE1 mode transmission is shown in Fig. 7 for an ultra-broadband combiner with a 300 μm coupler length. Both TE0 and TE1 modes are separately launched and each mode overlap integral with both TE0 and TE1 modes is measured for the transmission of the combiner.

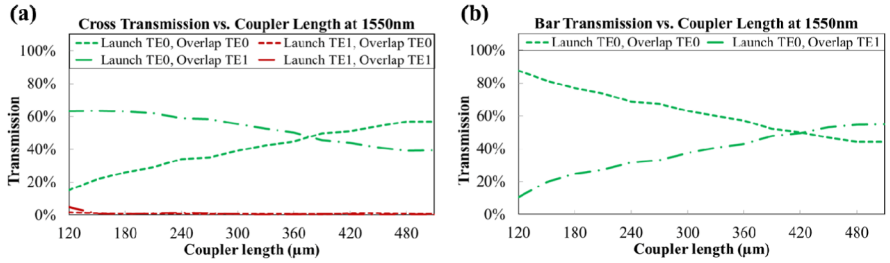

Fig. 7. Simulation launching TE0 and TE1 modes and measuring the overlap integral with the TE0 and TE1 modes at the output.

2.4 Ultra-broadband combiner fabrication

These devices are fabricated on silicon substrate wafers with 2 μm of thermally grown silicon dioxide. A 200 nm layer of low-pressure chemical vapor deposition (LPCVD) stoichiometric silicon nitride is deposited on top of the silicon dioxide and deep-UV lithography with carbon tetrafluoride and oxygen inductively coupled plasma (ICP) etching defines the waveguides. A second lithography and etch step defines the fully etched silicon nitride regions shown in Fig. 5. Finally, a 2 μm plasma-enhanced chemical vapor deposition (PECVD) silicon dioxide layer forms the top cladding layer and the wafer is annealed at 1050°C for 8 hours to improve silicon dioxide index uniformity. An optical photograph in Fig. 8 shows devices and polished facets of 2 out of the 1680 devices processed on one 4-inch wafer. The device yield was 100% for the 90 measured devices. Etched channels in the cladding silicon dioxide, visible along the side of the coupler in Fig. 7, are unused in this work, but allow for future investigation of an undercut substrate to reduce substrate leakage loss of the mid-IR band wavelengths.

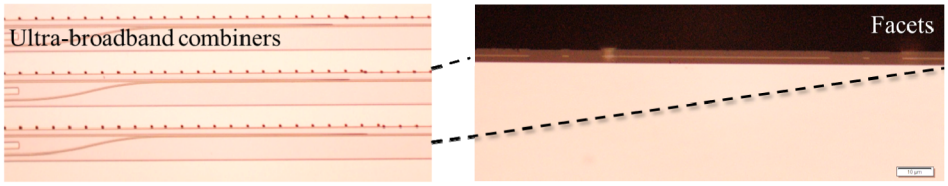

Fig. 8. Microscope picture of fabricated ultra-broadband combiners top view and facet view.

3. Experimental setup

Insertion losses were measured in three different wavelength bands to demonstrate ultra-broadband operation. A tunable laser at 780 nm is used as the VNIR source. An incoherent broadband light source with peaks at 1310 nm, 1430 nm, and 1550 nm is used as the NIR source. An interband cascade laser (ICL) at 3600 nm is used at the mid-IR source. Figure 9 shows the measurement setup schematics for the (V)NIR measurements and the mid-IR measurements. Both setups free space couple light from a source to the input waveguide. High TE polarized input with polarization extinction ratio >45 dB is ensured for the (V)NIR setup in Fig. 9(a) with a dichroic film polarizer. The mid-IR setup in Fig. 9(b) has a high polarization extinction ratio of >20 dB due to the lasing polarization in the ICL. The output

#230667 - $15.00 USD Received 16 Jan 2015; revised 20 Mar 2015; accepted 20 Mar 2015; published 22 Apr 2015
© 2015 OSA

waveguide couples light into a single mode fiber and the output of the fiber is measured by a photodetector.

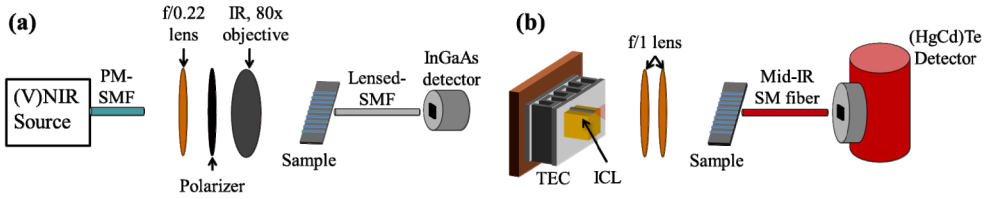

Fig. 9. Measurement setup for (a) NIR and (b) mid-IR insertion losses.

4. Measurement results

The ultra-broadband combiner is designed to operate in regions of high fundamental mode transmission. The first measurement result subsection 4.1 reports two demonstrations of the high transmission region with VNIR and mid-IR wavelength transmission data. For the cross-over wavelength region, reported in the second subsection 4.2, the NIR transmission data shows transmission trends as a function of coupler length, indicating that the cross-over wavelength changes with coupler length.

4.1 High transmission regimes

The fundamental mode transmission is measured for coupler lengths from 120 μm to 510 μm in steps of the 30 μm. For VNIR, high transmission near 100% is shown invariant of coupler length in Fig. 10(a), which matches the overlaid simulation trend. The transmission data is normalized to the transmission from a device with the same input and output waveguides as the ultra-broadband combiner, but with only a straight or tapered waveguide in between. Only the device insertion loss is presented since the input and output coupling losses, material absorption losses, waveguide scattering loss, and waveguide bend losses are all normalized.

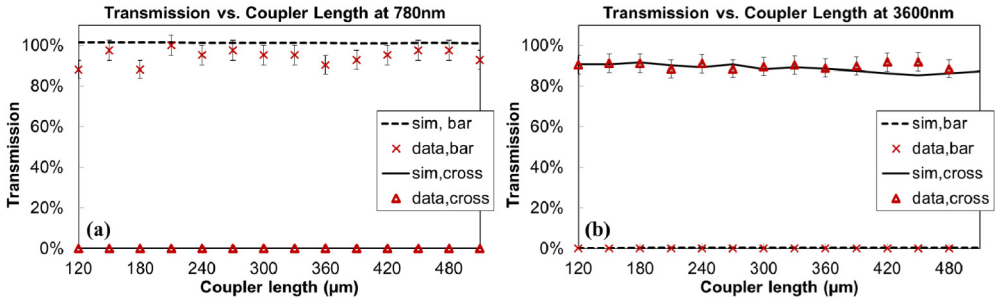

Fig. 10. Transmission vs. coupler length for (a) 780 nm wavelength bar input and (b) 3600 nm wavelength cross input including overlaid BPM simulated transmission for each. RMS error of 5% is represented by error bars.

For mid-IR, the normalized transmission for each coupler length is shown in Fig. 10(b), where the simulation data is overlaid. The high transmission invariant of coupler length agrees with the simulation data. By measuring series of identical devices, an RMS error is calculated as 5% for the normalized data in both VNIR and mid-IR measurements.

4.2 Cross-over wavelength regime

Fundamental mode transmission data for the 1310 nm, 1430 nm, and 1550 nm bands show the complete trend of high to low and low to high transmission through the cross-over wavelength from the bar and cross inputs, respectively. The 1310 nm measurements in Fig. 11(a) show high transmission from the bar input, decreasing as coupler length increases, and low

#230667 - $15.00 USD Received 16 Jan 2015; revised 20 Mar 2015; accepted 20 Mar 2015; published 22 Apr 2015
© 2015 OSA

transmission from the cross input, increasing as coupler length increases. This indicates that 1310 nm is shorter than the cross-over wavelength.

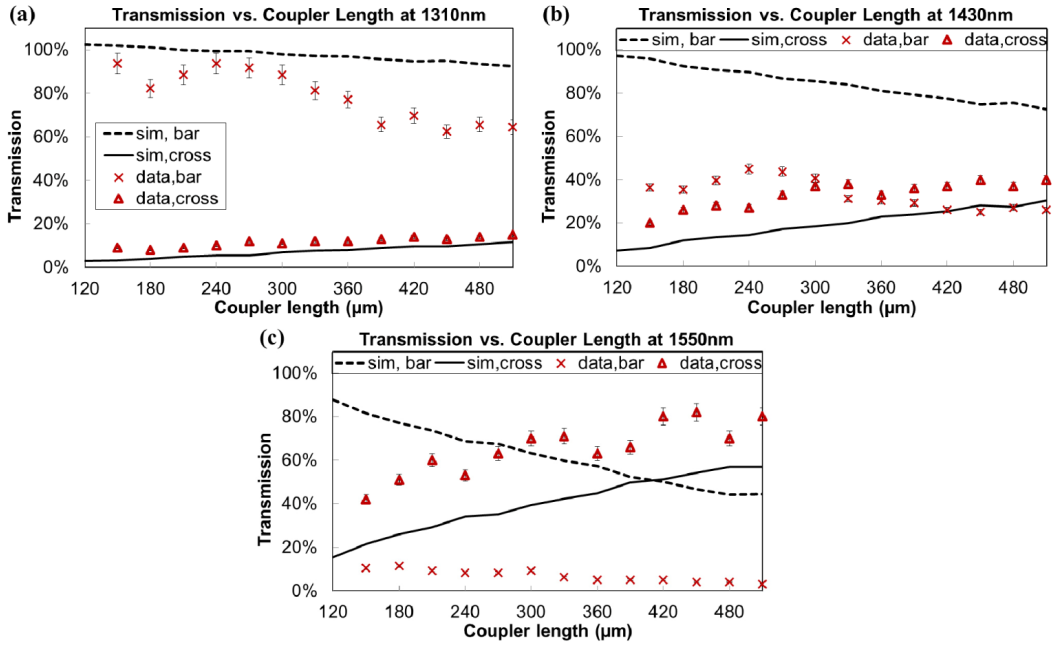

Fig. 11. Transmission vs. coupler length for (a) 1310 nm, (b) 1430 nm, and (c) 1550 nm wavelengths in the bar and cross inputs including overlaid BPM simulated transmission in (c).

Measurements in Fig. 11(b) show equivalent transmission at 300 μm, indicating the cross-over wavelength is near 1430 nm. Fundamental mode transmission in Fig. 11(c) shows a trend of increasing cross transmission with increasing coupler length and decreasing bar transmission with increasing coupler length suggesting the cross-over wavelength is shorter than 1550 nm. Although data in Fig. 11 does not match corresponding simulations, the trends indicate the dependence of cross-over wavelength to coupler length and a cross-over wavelength shift. Section 5 discusses hypotheses for this discrepancy.

4.3 Ultra-broadband transmission spectrum

By putting transmission data from each spectral band measurement together from a single coupler length, the transmission spectrum of the ultra-broadband coupler is shown in Fig. 12 for the bar and cross input excitations. The VNIR and mid-IR data points show high transmission as predicted and the cross-over wavelength is about 1430 nm, as shown from the NIR measurements. As simulations suggest, the VNIR cross transmission and the mid-IR bar transmission are low and these data points are both lower than the measurement dynamic range, which is 35 dB for the NIR setup and 30 dB for the mid-IR setup.

#230667 - $15.00 USD Received 16 Jan 2015; revised 20 Mar 2015; accepted 20 Mar 2015; published 22 Apr 2015
© 2015 OSA

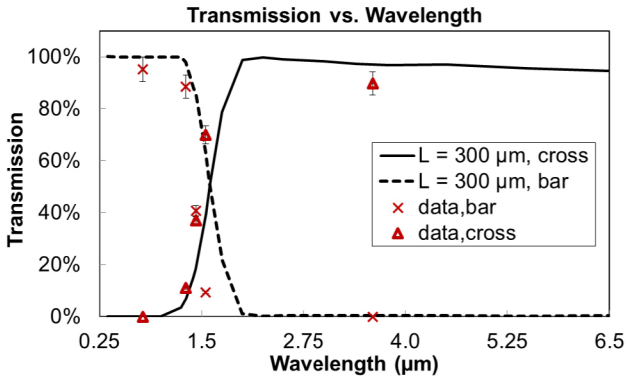

Fig. 12. Transmission vs. wavelength for 300 μm coupler length in the bar and cross inputs including overlaid BPM simulated transmission.

5. Discussion

Although the measured transmission above and below the cross-over wavelength corresponds well with the BPM simulation, Fig. 12 shows the measured cross-over wavelength is blue-shifted relative to simulations. Also, the slope of transmission versus wavelength is steeper near the cross-over wavelength for both cross and bar inputs. At the cross-over wavelength in Fig. 11, it is evident that the sum of the measured cross and bar fundamental mode transmission is less than the sum of the simulated cross and bar fundamental mode transmission. Therefore, either more light is coupled into the higher order mode or the light is scattering at this wavelength. A number of fabrication related issues could have affected these discrepancies including the formation of air gaps and strain from PECVD top cladding deposition, affecting the material indices, which were not accounted for in this simulation. Air gaps did develop from the PECVD top cladding deposition at the waveguide facets, but air gaps were no longer visible in SEM images after the anneal. Further analysis to dice and polish the devices will reveal if air gaps still exist along the coupler.

Another factor that affects the accuracy of the measurement data is how much the measurement data represents the fundamental mode transmission. Especially in the cross-over wavelength regime, the higher order TE mode becomes excited in the coupler and can skew the measurement data if the TE1 mode has a high overlap integral with the output coupling, which can be increased if the fiber is not aligned to the geometric center of the waveguide. An incoherent broadband source is used for the NIR measurement and alignment to the waveguide center is ensured by monitoring the output spectrum. If the normalized spectrum flat, then the fiber is aligned to the waveguide center since higher order modes are least excited and mode beating is minimized. Since the input and output coupling are roughly Gaussian shapes with $1/e^2$ width of 2 μm, the overlap integral with the TE0 and TE1 modes is calculated to be 94% and 6%, respectively, for a fiber aligned to the center of the waveguide. Using the mode transmission results incorporating the TE0 and TE1 modes from Table 1 and Fig. 7, the transmission for a 300 μm long coupler is predicted to be 58.8% including normalization compared to the fundamental mode simulated transmission of 63.2% for the bar input. For the cross input the normalized transmission including both modes is 42.8% compared to the fundamental mode simulated transmission of 39.3%. These predicted values are only 4.4% point higher and 3.5% point lower, respectively. Although this is a relatively small error in transmission, this would result in a blue-shift of the cross-over wavelength relative to the fundamental mode simulations shown in Fig. 12. Therefore, the higher order TE mode excitation does contribute to the cross-over wavelength blue-shift by approximately 15 nm. This shift is small compared to the measured shift of about 160 nm so this error is not the only factor contributing to the cross-over wavelength shift.

#230667 - $15.00 USD Received 16 Jan 2015; revised 20 Mar 2015; accepted 20 Mar 2015; published 22 Apr 2015
© 2015 OSA

Since higher order modal excitation does not contribute all of the cross-over wavelength error, we hypothesize that possible air gaps and strain have significantly altered the material indices to cause this discrepancy. Both air gaps and altered indices could contribute to higher order mode coupling, explaining the decrease in fundamental mode transmission at the cross-over wavelength. Since strain affects are not likely isotropic, further three dimensional analysis of strain in this design is necessary to characterize the possible effects of strain on the cross-over wavelength shift.

6. Conclusion

A feasible design for an integrated multi-octave spectral beam combiner design has been presented including a novel ultra-broadband combiner. We have also demonstrated high transmission greater than 90% for 780 nm and 3600 nm wavelengths, and we have shown the existence of the cross-over wavelength at NIR, although it was spectrally shifted relative to the simulation results. This technology uses an ultra-broadband platform compatible with previously demonstrated spectral combining technologies and lasers bonded to silicon. It is now feasible to envision an integrated array of lasers spanning UV to mid-IR bands spectrally combined into a single output waveguide for high power and ultra-broadband applications.

Acknowledgments

We thank Jared F. Bauters, Michael L. Davenport, and Vincent K. Komala for helpful discussions and Jerry R. Meyer for providing the interband cascade laser. This work is being supported by the U.S. Office of Naval Research (ONR) under the Grant Number N00014-13-C-0147.

#230667 - $15.00 USD Received 16 Jan 2015; revised 20 Mar 2015; accepted 20 Mar 2015; published 22 Apr 2015
© 2015 OSA